

RESEARCH REPORT

The effect of size, charge, and peptide ligand length on kidney targeting by small, organic nanoparticles

Yi Huang¹ | Kairui Jiang¹ | Xuting Zhang¹ | Eun Ji Chung^{1,2,3,4} ¹Department of Biomedical Engineering, University of Southern California, Los Angeles, California²Department of Chemical Engineering and Materials Science, University of Southern California, Los Angeles, California³Department of Medicine, Division of Nephrology and Hypertension, University of Southern California, Los Angeles, California⁴Department of Surgery, Division of Vascular Surgery and Endovascular Therapy, University of Southern California, Los Angeles, California**Correspondence**

Eun Ji Chung, Department of Biomedical Engineering, University of Southern California, 1002 Childs Way, MCB 357, Los Angeles, CA 90089.

Email: eunchung@usc.edu

Funding information

Gabilan Assistant Professorship; L. K. Whittier Foundation; NIH New Innovator Award, Grant/Award Number: DP2-DK121328; The National Heart, Lung, and Blood Institute, Grant/Award Number: R00HL124279; Women in Science and Engineering (WISE), University of Southern California

Peer ReviewThe peer review history for this article is available at <https://publons.com/publon/10.1002/btm2.10173>.**Abstract**

Chronic kidney disease (CKD) affects 15% of the US adult population. However, most clinically available drugs for CKD show low bioavailability to the kidneys and non-specific uptake by other organs which results in adverse side effects. Hence, a targeted, drug delivery strategy to enhance kidney drug delivery is highly desired. Recently, our group developed small, organic nanoparticles called peptide amphiphile micelles (PAM) functionalized with the zwitterionic peptide ligand, (KKEEE)₃K, that passage through the glomerular filtration barrier for kidney accumulation. Despite high bioavailability to the kidneys, these micelles also accumulated in the liver to a similar extent. To further optimize the physicochemical properties and develop design rules for kidney-targeting micelles, we synthesized a library of PAMs of varying size, charge, and peptide repeats. Specifically, variations of the original (KKEEE)₃K peptide including (KKEEE)₂K, (KKEEE)K, (EEKKK)₃E, (EEKKK)₂E, (EEKKK)E, KKKKK, and EEEEE were functionalized onto nanoparticles, and peptide surface density and PEG linker molecular weight were altered. After characterization with transmission electron microscopy (TEM) and dynamic light scattering (DLS), nanoparticles were intravenously administered into wildtype mice, and biodistribution was assessed through ex vivo imaging. All micelles localized to the kidneys, but nanoparticles that are positively-charged, close to the renal filtration size cut-off, and consisted of additional zwitterionic peptide sequences generally showed higher renal accumulation. Upon immunohistochemistry, micelles were confirmed to bind to the multiligand receptor, megalin, and histological analyses showed no tissue damage. Our study provides insight into the design of micelle carriers for kidney targeting and their potential for future therapeutic application.

KEYWORDS

chronic kidney disease, micelle, nanoparticle, peptide, renal clearance

1 | INTRODUCTION

Chronic kidney disease (CKD) affects 600 million people globally and is characterized by gradual kidney function decline.¹ A common form

of CKD is autosomal dominant polycystic kidney disease (ADPKD), which affects over 12 million people worldwide and is characterized by renal cyst formation that can result in the need for dialysis or kidney transplant.²⁻⁵ Currently, there is no cure for ADPKD and

This is an open access article under the terms of the Creative Commons Attribution License, which permits use, distribution and reproduction in any medium, provided the original work is properly cited.

© 2020 The Authors. *Bioengineering & Translational Medicine* published by Wiley Periodicals LLC on behalf of American Institute of Chemical Engineers.

tolvaptan is the only FDA approved treatment for ADPKD.⁶ Despite enthusiasm, tolvaptan has been reported to cause several side effects including polyuria, thirst, nocturia, and drug-induced liver damage.⁷⁻¹⁰ According to a study of 961 ADPKD patients undergoing tolvaptan treatment, the adverse event rates for thirst and nocturia were found to be approximately 55% and 29%.⁹ Polyuria affected 38% of patients and was the primary reason for dose reduction and drug discontinuation due to its significant impact on patients' quality of life.^{11,12} Moreover, tolvaptan is known to cause liver toxicity and elevated liver enzyme levels, which may further deteriorate liver health, as liver cysts and fibrosis are common extrarenal manifestations of ADPKD.^{8,13} As a result, frequent monitoring of liver function is required for patients on tolvaptan treatment.^{14,15} Like tolvaptan, many drugs for CKD lead to non-specific uptake and undesired adverse effects,^{16,17} and hence, the development of a targeted drug delivery platform that can directly unload drugs to diseased kidneys has the potential to reduce systemic side effects without compromising therapeutic efficacy.

To that end, our group has recently developed small, organic nanoparticles called peptide amphiphile micelles (PAMs, ~15 nm in diameter) to target the kidneys by incorporating the zwitterionic peptide ligand, (KKEEE)₃K([Lys-Lys-Glu-Glu-Glu]₃-Lys), which has been found to bind to megalin, a multiligand receptor highly expressed on renal proximal tubule cells.¹⁸⁻²⁰ Upon intravenous injection of (KKEEE)₃K PAMs into wildtype mice, although (KKEEE)₃K PAMs were found to accumulate in the kidneys to a high degree, they also accumulated similarly in the liver, likely due to the mononuclear phagocytic system (MPS).¹⁹

The kidneys filter blood and each kidney is composed of approximately a million functional units called nephrons. Each nephron consists of two main parts, the renal tubule and the renal corpuscle which contains a network of blood capillaries called the glomerulus. When blood enters the glomerulus, a fraction of blood plasma will pass through the glomerular filtration barrier (GFB) and into the renal tubule system to be processed into urine (Figure 1).²¹ Specifically, the GFB is comprised of three components and includes the endothelium, glomerular basement membrane (GBM), and podocyte foot processes that collectively acts as a size-selective and charge-selective sieve during the filtration of macromolecules.²¹⁻²³ The pores present in each of these layers include fenestrations of the endothelium (70-90 nm), a mesh created through a network of collagen, laminin, and proteoglycans that make up the GBM (~8 nm), and filtration slits of the podocyte foot processes (4-11 nm).^{21,24} Regarding charge, both the endothelium and podocytes express glycocalyx on their membranes, mostly in the form of heparan sulfate (over 50%), which is negatively-charged.²⁵⁻²⁷ The GBM is also negatively-charged due to the presence of anionic proteoglycans (e.g., heparan-sulfate and chondroitin-sulfate glycosaminoglycan), and hence, positively-charged nanoparticles have been reported to pass through the GFB more readily due to charge repulsion upon interaction with negatively-charged macromolecules.^{28,29}

While most nanoparticles are too large to cross the fenestration of the GFB and will be recognized by the MPS system, ultrasmall

nanoparticles (<8 nm) have been reported to pass through the GFB and clear via renal clearance.³⁰ Since the majority of cyst development in CKD such as PKD occurs in the tubules,^{31,32} one strategy for targeted drug delivery for PKD is to design nanoparticles that can pass through the GFB through their physicochemical properties, but be retained in proximal tubule through the addition of targeting ligands. Hence, to study how size, charge, peptide ligand length, and surface ligand density affects nanoparticle kidney-targeting ability and to optimize the kidney-targeting potential of PAMs, we developed a library of micelles by incorporating variations of the original zwitterionic (KKEEE)₃K peptide including (KKEEE)₂K, (KKEEE)K, (EEKKK)₃E, (EEKKK)₂E, (EEKKK)E, KKKKK, and EEEEE. The size and surface charge of the micelle library was characterized by TEM, DLS, and zeta potential, and to assess nanoparticle kidney-targeting ability, micelles were intravenously administered into C57B/6J mice. Kidney targeting and micelle biodistribution was evaluated via ex vivo imaging after 24 hours. Moreover, micelle targeting to megalin was evaluated through immunohistochemistry, and kidney biocompatibility was assessed through histology, blood urea nitrogen, and urine creatinine.

2 | RESULTS AND DISCUSSION

2.1 | Synthesis and characterization of PAMs

The kidney-targeting peptide (KKEEE)₃K was found to accumulate in the kidneys in part by binding to the megalin receptor expressed on proximal tubule cells and is composed of three repeats of the peptide sequence, KKEEE.¹⁹ Previously, when (KKEEE)₃K was incorporated into micelles and assessed in vivo, their biodistribution profile showed enhanced kidney accumulation but also liver accumulation of 35% likely due to the MPS system as (KKEEE)₃K PAMs were 15 nm in diameter and larger than the cut off reported for passage through the GFB (8-10 nm).¹⁹ To optimize the physicochemical properties of PAMs, herein, we synthesized micelles with fewer repeats of KKEEE to test how peptide repeat number affected kidney accumulation. Moreover, since micelles are self-assembled from monomers containing DSPE hydrophobic tails linked to polyethylene glycol (PEG), PEG molecular weight was also varied to further study the size effects on the renal targeting ability of nanoparticles. In addition to peptide repeat number and size, peptide sequences of opposite charge (e.g., EEKKE) as well as non-zwitterionic peptide sequences (e.g., KKKKK and EEEEE) were incorporated to test the charge selectivity of the GFB on micelles. Furthermore, to assess how peptide ligand surface density affects renal targeting ability, we synthesized micelles with 50% or 100% peptide surface presentation.

To characterize the micelles, PAMs were self-assembled in water or PBS at 100 μM (which is above the critical micelle concentration of ~1 μM³³) and assessed via TEM and DLS. TEM images demonstrated spherical morphology of all PAMs (Figure 2), and DLS confirmed that decreasing the number of KKEEE repeats on nanoparticles correlated with a slight decrease in hydrodynamic diameter, although the diameter of all micelles were close in range to one another:

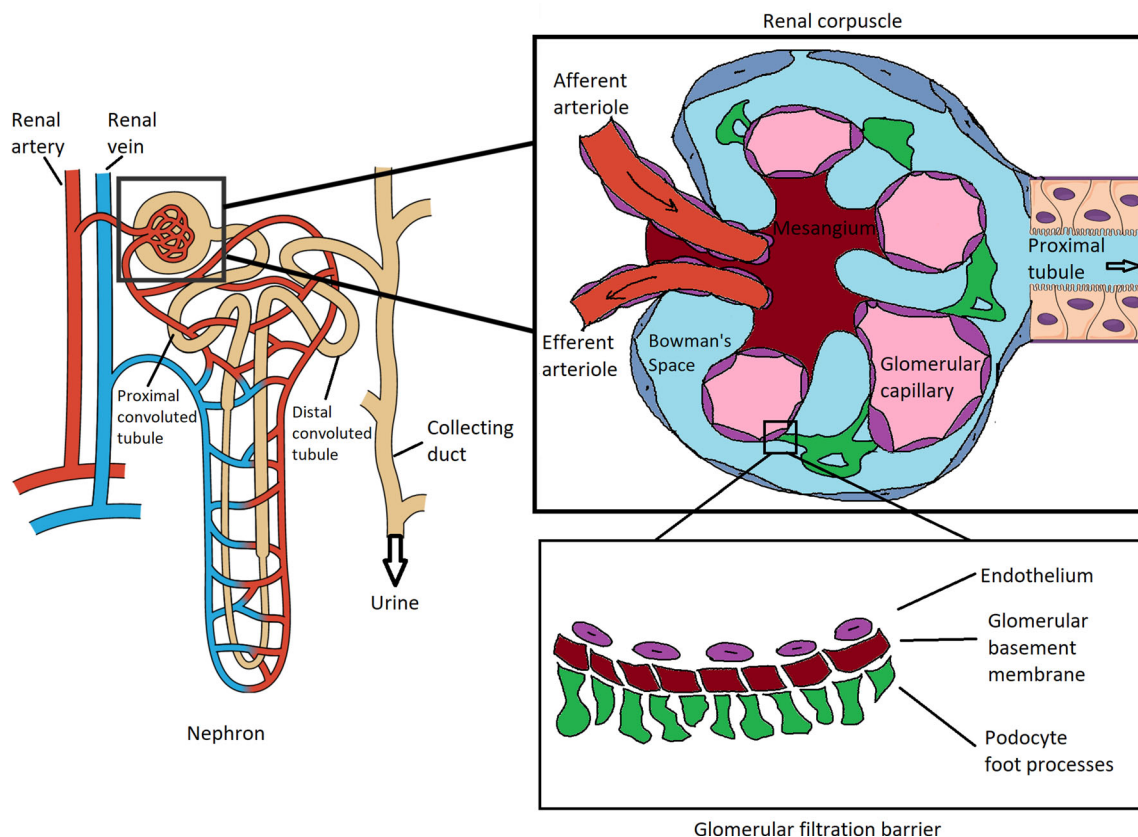


FIGURE 1 Schematic of the nephron, renal corpuscle, and the glomerular filtration barrier

PEG2000-(KKEEE)₃K (16.6 ± 2.5 nm), PEG2000-(KKEEE)₂K (12.2 ± 0.6 nm), PEG2000-(KKEEE)K (10.6 ± 1.7 nm); PEG2000-(EEKKK)₃E (12.4 ± 1.2 nm), PEG2000-(EEKKK)₂E (14.0 ± 1.8 nm), PEG2000-(EEKKK)E (11.8 ± 1.5 nm). PEG2000-KKKKK and PEG2000-EEEE had an average diameter of 11.2 ± 1.2 nm and 10.2 ± 1.3 nm, which were similar to PEG2000-(KKEEE)K and PEG2000-(EEKKK)E due to the shorter peptide sequence (Table 1, Figure S1). As expected,³⁴ increasing the PEG molecular weight to 5,000 resulted in a slight increase in diameter of nanoparticles to 17.2 ± 1.8 nm, and nanoparticles consisting of DSPE-PEG1000 had a diameter of 10.4 ± 1.8 nm (Table 1).

Interestingly, despite (KKEEE)₃K and (EEKKK)₃E having an opposite net charge of −2 and +2 derived from additional negatively-charged glutamic acid (E) or positively-charged lysine (K), the zeta potential of both micelles were found to be near neutral at −0.6 ± 1.4 mV and 0.03 ± 0.1 mV, respectively (Table 1). Similarly, the zeta potentials of PEG2000-(KKEEE)₂K (net −1), PEG2000-(EEKKK)₂E (net +1), PEG2000-(KKEEE)K (net 0), and PEG2000-(EEKKK)E (net 0) were also found to be near neutral at −0.2 ± 0.3 mV, −3.1 ± 6.4 mV, −1.1 ± 0.6 mV, and −0.1 ± 0.7 mV. Since all these micelles consisted of 50:50 molar ratio of peptide-DSPE-PEG2000 to DSPE-PEG2000-methoxy, it is possible that the near-neutral charge of DSPE-PEG2000-methoxy amphiphiles masked any charge differences of the micelles resulting in neutral zeta potentials. As the zeta potential of DSPE-PEG2000-NT (consisting of 100% DSPE-PEG2000-methoxy)

was found to be near neutral (−3.2 ± 5.4 mV), the addition of 50% molar ratio of DSPE-PEG2000-methoxy may have affected their surface charge, leading to the resultant near-neutral zeta potential measurements of PEG2000-(KKEEE)₃K and PEG2000-(EEKKK)₃E. This was also the case with nanoparticles consisting of 50% KKKKK, which had a zeta potential of 0.07 ± 0.2 mV (Table 1). On the other end, when the peptide sequence was altered to 50% EEEEE, micelles consisted of a negative zeta potential of −40.9 ± 4.6 mV.

Given these results, we synthesized micelles consisting of entirely PEG2000-(KKEEE)₃K and PEG2000-(EEKKK)₃E. Zeta potential measurements of 100% PEG2000-(KKEEE)₃K and 100% PEG2000-(EEKKK)₃E micelles were found to be −41.4 ± 2.9 mV and 14.3 ± 1.6 mV, which is more consistent with the net charge of peptide sequence, −2 and +2, respectively (Table 1).

2.2 | In vivo renal targeting and biodistribution

To test the effects of nanoparticle characteristics on renal targeting, Cy7-labeled micelles were intravenously administered into 6–7 week old male and female C57B/6 J mice and after 24 hours, micelle accumulation was assessed via ex vivo imaging of the kidneys, brain, lung, heart, liver, spleen, intestine, and bladder. 10 mol% of Cy7 was included into micelles to maximize the fluorescence signal without quenching and micelles with 45:45:10 molar ratio of DSPE-PEG-methoxy:

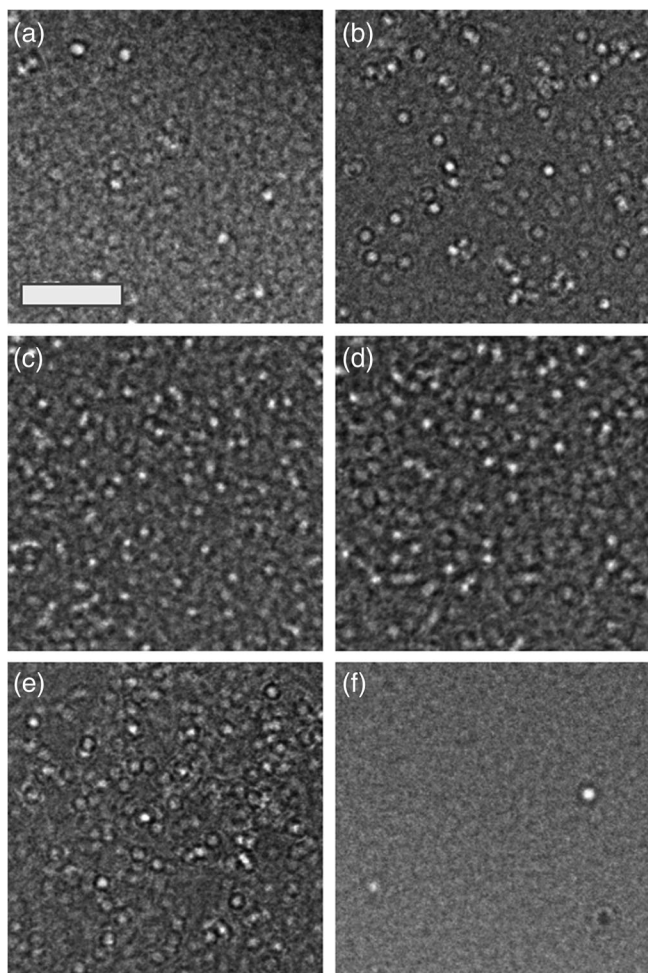


FIGURE 2 TEM images of micelles. (a) 50% PEG2000-(KKEEE)₃K, (b) 50% PEG2000-(EEKKK)₃E, (c) 50% PEG2000-KKKKK, (d) 50% PEG2000-EEEE, (e) 50% PEG1000-(KKEEE)₃K, and (f) 100% PEG5000-(KKEEE)₃K show spherical morphology. Scale bar: 100 nm

DSPE-PEG-peptide:DSPE-PEG-Cy7 or 90:10 molar ratio of DSPE-PEG-peptide:DSPE-PEG-Cy7 were synthesized for *in vivo* studies.³⁵ As shown in Figure S2, despite all micelles being at or above the reported renal filtration cut-off size, all micelles accumulated in the kidneys to a greater extent than all other organs with the exception of 90% PEG5000-(KKEEE)₃K (Figure S2).¹⁹ 90% PEG5000-(KKEEE)₃K, which had the highest PEG molecular weight and largest diameter of 17.2 ± 1.8 nm (Table 1), mostly accumulated in the liver ($1.6 \times 10^9 \pm 1.3 \times 10^8$ p/s/cm²/sr) likely via recognition of the MPS system (Figure S3). However, this was not statistically significant with its accumulation in the kidneys, which indicates an ability to simultaneously pass through the GFB and accumulate in the kidneys (Figures S2 and S3). Although the size of micelles was slightly larger than the cut-off diameter of glomerular filtration (~10 nm), kidney accumulation and passage through the GFB has been found for 60–100 nm polycation-siRNA nanoparticles and other soft macromolecules with the diameter beyond the cut-off size of 8–10 nm.^{24,36}

2.2.1 | Biodistribution of PAMs with varying number of peptide repeats

In Figure 3a, the effect of KKEEE/EEKKK repeats on nanoparticle kidney targeting *in vivo* was evaluated. Although we hypothesized that peptides with fewer repeats of KKEEE/EEKKK would decrease the overall molecular weight and size of micelles and thereby improve the ability of nanoparticles to pass through the GFB and accumulate in the kidneys, as shown in Figure 3a, additional sequence repeats trended towards having higher renal accumulation. Specifically, for micelles with 45% peptide surface presentation, PEG2000-(KKEEE)₃K ($2.3 \times 10^9 \pm 3.7 \times 10^8$ p/s/cm²/sr) had the highest fluorescence intensity, followed by PEG2000-(KKEEE)₂K ($2.2 \times 10^9 \pm 3.3 \times 10^8$ p/s/cm²/sr) and PEG2000-(KKEEE)K ($1.8 \times 10^9 \pm 1.5 \times 10^8$ p/s/cm²/sr, Figure 3a, although not statistically significant). Similarly, for PAMs with EEKKK repeats, PEG2000-(EEKKK)₃E ($2.4 \times 10^9 \pm 2.7 \times 10^8$ p/s/cm²/sr) showed higher renal fluorescence intensity than PEG2000-(EEKKK)₂E ($1.7 \times 10^9 \pm 1.0 \times 10^8$ p/s/cm²/sr, $p < .01$). PEG2000-(EEKKK)E had a fluorescence intensity of $1.8 \times 10^9 \pm 1.9 \times 10^8$ p/s/cm²/sr, which was also statistically lower compared to PEG2000-(EEKKK)₃E ($p < .05$, Figure 3a). Given that KKEEE and EEKKK are zwitterionic peptides, one possible explanation for the higher kidney accumulation of micelles consisting of PEG2000-(KKEEE)₃K and PEG2000-(EEKKK)₃E micelles is that the additional peptide repeats provided enhanced zwitterionic characteristics and hence, resistance to nonspecific protein and opsonin absorption as well as liver uptake via the MPS system.^{37–42} Additionally, given that the hydrodynamic diameter of the micelles with varying peptide repeats fell within a narrow range (Table 1 and Figure S1), peptide sequence and ligand length may play a more important role in the renal accumulation of micelles rather than size, which will be further probed in future studies.

2.2.2 | Biodistribution of PAMs with opposite charge

In Figure 3b, we compared the charge effects on micelle renal targeting. Despite having an opposite net charge of -2 and $+2$, PEG2000-(KKEEE)₃K and PEG2000-(EEKKK)₃E with 45% surface peptide density accumulated in the kidneys to a similar extent ($2.3 \times 10^9 \pm 3.7 \times 10^8$ p/s/cm²/sr and $2.4 \times 10^9 \pm 2.7 \times 10^8$ p/s/cm²/sr, respectively, Figure 3b). As found in Table 1, the zeta potentials of both micelles were near neutral due to the incorporation of PEG2000-methoxy, which likely masked any charge differences that contributed to kidney targeting. Moreover, as mentioned, both peptides are zwitterionic and nanoparticles coated with zwitterionic materials have been reported to resist serum protein adsorption *in vivo* due to the highly hydrophilic surface and anti-fouling properties.^{43,44} On the other hand, micelles consisting of 90% PEG2000-(KKEEE)₃K, which had zeta potential of -41.4 ± 2.9 mV, had lower kidney accumulation ($1.8 \times 10^9 \pm 1.7 \times 10^8$ p/s/cm²/sr) than the positively-charged

TABLE 1 Characterization of PAMs by DLS and zeta potential

NP	Peptide surface density (%)	Diameter (nm)	Zeta potential (mV)	Net charge
PEG2000-(KKEEE) ₃ K	50	16.6 ± 2.5	-0.6 ± 1.4	-2
PEG2000-(KKEEE) ₂ K	50	12.2 ± 0.6	-0.2 ± 0.3	-1
PEG2000-(KKEEE)K	50	10.6 ± 1.7	-1.1 ± 0.6	0
PEG2000-(EEKKK) ₃ E	50	12.4 ± 1.2	0.03 ± 0.1	+2
PEG2000-(EEKKK) ₂ E	50	14.0 ± 1.8	-3.1 ± 6.4	+1
PEG2000-(EEKKK)E	50	11.8 ± 1.5	-0.1 ± 0.7	0
PEG2000-KKKKK	50	11.2 ± 1.2	0.1 ± 0.2	+5
PEG2000-EEEE	50	10.2 ± 1.3	-40.9 ± 4.6	-5
PEG2000-(KKEEE) ₃ K	100	10.6 ± 0.4	-41.4 ± 2.9	-2
PEG2000-(EEKKK) ₃ E	100	15.0 ± 0.4	14.3 ± 1.6	+2
PEG1000-(KKEEE) ₃ K	50	10.4 ± 1.8	-2.9 ± 2.9	-2
PEG5000-(KKEEE) ₃ K	100	17.2 ± 1.8	-9.6 ± 1.0	-2
PEG2000-NT	100	7.5 ± 0.1	-3.2 ± 0.8	0

(14.3 ± 1.6 mV) 90% PEG2000-(EEKKK)₃E ($2.4 \times 10^9 \pm 1.0 \times 10^8$ p/s/cm²/sr, $p < .05$). These results correlated with findings by Liang et al and Balogh et al that reported the GFB is a charge-selective barrier in which positively-charged nanoparticles pass through the GFB more easily than negatively-charged nanoparticles and macromolecules due to electrostatic repulsion of the GBM.⁴⁵⁻⁴⁸ In addition, 90% PEG2000-(KKEEE)₃K had significant higher liver uptake ($1.6 \times 10^9 \pm 5.0 \times 10^7$ p/s/cm²/sr) than 90% PEG2000-(EEKKK)₃E ($1.0 \times 10^9 \pm 9.9 \times 10^7$ p/s/cm²/sr, $p < .0001$, Figure S4). The higher liver uptake of negatively-charged 90% PEG2000-(KKEEE)₃K was similar to the results by Xiao et al that reported negatively-charged PEG-oligocholic acid based micellar nanoparticles (-26.9 ± 1.7 mV) have higher liver uptake than positively-charged counterparts (3.6 ± 0.8 mV) that were similar in size (18 ~ 21 nm).⁴⁹

2.2.3 | The effects of PEG molecular weight and size on the biodistribution of micelles

In Figure 3c, we evaluated how the size of nanoparticles alters kidney targeting and compared micelles with varying PEG molecular weight.⁵⁰ (KKEEE)₃K micelles consisting of PEG1000 had renal accumulation of $2.43 \times 10^9 \pm 2.0 \times 10^8$ p/s/cm²/sr that was significantly greater than (KKEEE)₃K micelles consisting of PEG5000 ($1.28 \times 10^9 \pm 2.3 \times 10^8$ p/s/cm²/sr, $p < .0001$, as 45% PEG1000-(KKEEE)₃K micelles were found to be 10.4 ± 1.8 nm in diameter and near the reported renal filtration cut-off size (Table 1, Figures 3c and 4). Similarly, PEG5000-(KKEEE)₃K showed lower renal accumulation compared to PEG20000-(KKEEE)₃K with 90% peptide density ($1.28 \times 10^9 \pm 2.3 \times 10^8$ p/s/cm²/sr and $1.8 \times 10^9 \pm 1.7 \times 10^8$ p/s/cm²/sr, respectively, $p < .0001$). Hence, our results demonstrate a negative correlation between the size and renal targeting ability of PAMs.

The potential influence of the protein corona on micelles on GFB penetration will be further studied in the future to better understand the factors that affect nanoparticle kidney targeting.

2.3 | Micelle colocalization with megalin

As mentioned, previously, the (KKEEE)₃K peptide was found to target the kidney in part through megalin, a multiligand receptor that is present on the plasma membrane of proximal tubule cells, and the (KKEEE)₃K peptide showed significantly reduced uptake in megalin-deficient mice.^{19,20,51-53} As demonstrated by Vegt et al, megalin has been reported to associate with a library of peptides (octreotide, octreotate, minigastrin, exendin, and neurotensin) of varying charges.⁵⁴ To verify micelle binding to megalin, immunohistochemistry staining of kidneys of mice treated with 45% PEG2000-(KKEEE)₃K as well as 45% PEG2000-(EEKKK)₃E were assessed, and colocalization was calculated. A similar Pearson's *R* value, corresponding to colocalization, of 45% PEG2000-(EEKKK)₃E (0.53 ± 0.02) to megalin was shown with 45% PEG2000-(KKEEE)₃K (0.48 ± 0.04, not statistically significant) vs. the NT micelle (0.37 ± 0.03, $p < .01$, Figure 5), confirming that in addition to (KKEEE)₃K PAMs, PAMs consisting of zwitterionic peptides of opposite charge also accumulate in the kidneys in part via megalin. This corresponds with the ex vivo results that showed 45% PEG2000-(EEKKK)₃E had similar kidney accumulation to 45% PEG2000-(KKEEE)₃K (Figure 3a).

2.4 | Tissue morphology and kidney health

To assess the safety and biocompatibility of micelles and their eventual application as drug delivery vehicles, after ex vivo imaging, the brain, lung, heart, liver, spleen, intestine, kidney, and bladder were stained with H&E. In agreement with other PAM reports, the tissue morphology of all organs including the liver, intestine, and kidneys, where PAMs mostly accumulated, showed no tissue damage, and no significant difference was found to the PBS treatment group (Figure 6).^{19,55-59}

Kidney health and function of all the mice treated with micelles were further evaluated by assessing blood urea nitrogen (BUN) and urine

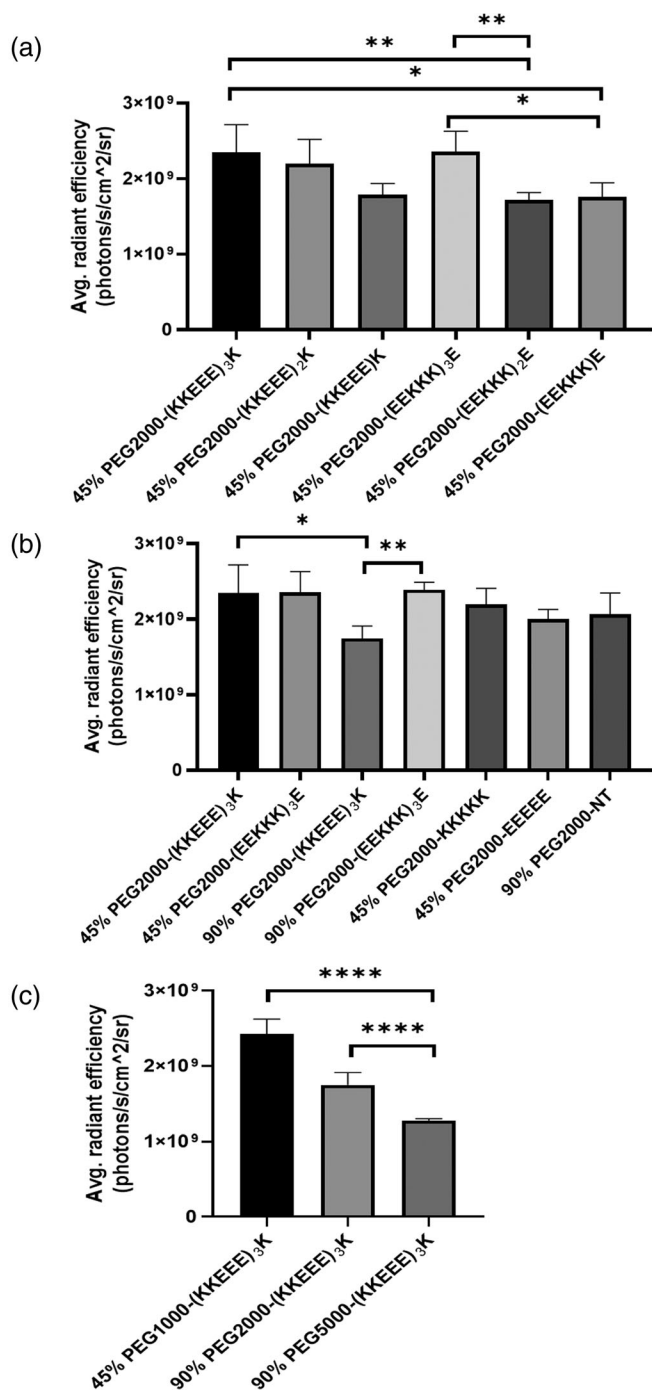


FIGURE 3 Kidney accumulation of micelles upon intravenous administration after 24 hours. Comparison of micelles containing (a) varying number of peptide repeats of KKEEE or EEKKE, (b) charge differences, and (c) (KKEEE)₃K with various PEG molecular weight. $n = 4$. * $p < .05$, ** $p < .01$, **** $p < .0001$

creatinine levels. BUN levels for C57BL/6 mice with healthy kidney function is 25.0–75.0 mg/dl,⁶⁰ and all the groups in this study were found to have BUN levels within this healthy range (Table 2). Similarly, the creatinine concentration in the urine indicates kidney health and urine creatinine levels for all groups were measured and found to fall within the healthy range for C57BL/6 mice (4.7 ± 3.1 mg/dl, Table 2).⁶¹

3 | CONCLUSION

In this study, we altered the physicochemical properties of PAMs by developing a library of micelles containing various peptide sequences and molecular weight and assessed its effect on renal targeting. Micelles were first characterized by TEM and DLS before intravenous administration into wildtype mice. After 24 hours post-administration, ex vivo imaging was conducted to compare kidney targeting ability. All PAMs tested in this study had high kidney accumulation, and our studies showed that nanoparticles with more zwitterionic amino acid repeats that are positively-charged and close to the renal filtration cut-off size tend to have higher renal accumulation. Furthermore, histological analyses confirmed no tissue damage, and kidney function levels of mice were within normal ranges. Overall, our studies indicate the potential of PAMs as targeting, nanocarriers for kidney applications and future work will focus on evaluating the mechanical properties and micelle concentration of nanoparticles on kidney targeting, as well as the influence of the protein corona on GFB penetration.⁶² Moreover, the therapeutic efficacy of drug-loaded micelles and the contribution of nanoparticle delivery through the peritubular capillaries will be assessed in CKD mouse models.

4 | MATERIALS AND METHODS

4.1 | Micelle synthesis

Peptides were synthesized using standard Fmoc-mediated solid phase peptide synthesis on an automatic PS3 peptide synthesizer (Protein Technologies, Tucson, AZ) with rink Amide resin (Protein Technologies, Tucson, AZ). A cysteine was added to the N-terminus of all the peptide sequences in order to make a thioether linkage reaction. The peptides were then cleaved from the resin with 94:2.5:2.5:1 volume ratios of trifluoroacetic acid:1,2-ethanedithiol:H₂O:triisopropylsilane. Cleaved peptides were precipitated and washed several times with ice cold diethyl ether, dissolved in Milli-Q water, lyophilized, and stored at -20°C . The crude peptides were purified by reverse-phase high performance liquid chromatography (HPLC) (Shimadzu, Kyoto, Japan) on a C18 column (Phenomenex, Torrance, CA) at 55°C with 0.1% formic acid in acetonitrile/water mixture. The purified peptides were characterized using matrix-assisted laser desorption ionization time-of-flight mass spectral analysis (MALDI-TOF) (Autoflex speed, Bruker, Billerica, MA) and conjugated to 1,2 distearoyl-sn-glycero-3-phosphoethanolamineN-[maleimide(polyethylene glycol)-1000/2000/5000], or DSPE-PEG (1000)-maleimide/DSPE-PEG(2000)-maleimide/DSPE-PEG(5000)-maleimide (Avanti Polar Lipids, Alabaster, AL) via a thioether linkage by mixing an equimolar amount of the lipid and pure peptide in Milli-Q water (pH 7.2) at room temperature for over 24 hours with gentle agitation. The mixture was further purified by a C4 column (Phenomenex, Torrance, CA) and characterized by MALDI-TOF as described above. The fluorophore-conjugated monomer was synthesized by mixing an equimolar amount of Cyanine7 NHS ester (Lumiprobe, Hunt Valley, MD) with 1,2-distearoyl-sn-glycero-3-phosphoethanolamineN-[amino (polyethylene glycol)-1000/2000/5000] (ammonium salt) or DSPE-PEG

FIGURE 4 Ex vivo images of kidney fluorescence after (a) 45% PEG2000-(KKEEE)₃K, (b) 45% PEG2000-(KKEEE)₂K, (c) 45% PEG2000-(KKEEE)K, (d) 45% PEG2000-(EEKKK)₃E, (e) 45% PEG2000-(EEKKK)₂E, (f) 45% PEG2000-(EEKKK)E, (g) 45% PEG2000-KKKKK, (h) 45% PEG2000-EEEE, (i) 90% PEG2000-(KKEEE)₃K, (j) 90% PEG2000-(EEKKK)₃E, (k) 45% PEG1000-(KKEEE)₃K, (l) 90% PEG5000-(KKEEE)₃K, (m) 90% PEG2000-NT, or (n) PBS administration at 24 hours

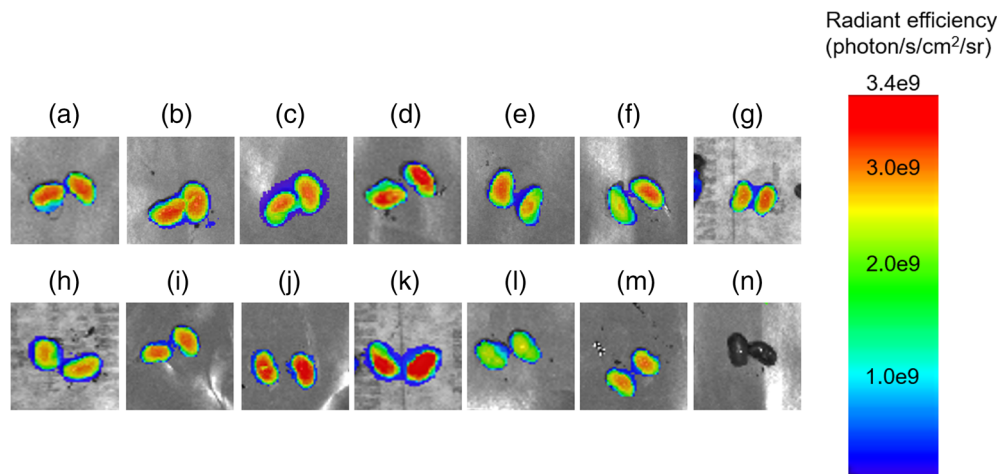
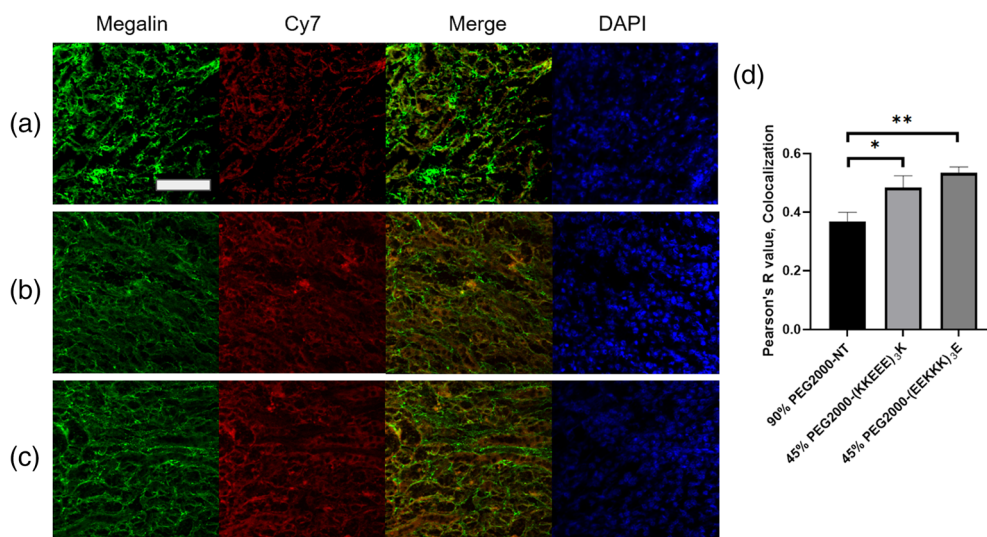


FIGURE 5 Megalin staining and colocalization with micelles in kidney section of mice administered (a) 90% PEG2000-NT, (b) 45% PEG2000-(KKEEE)₃K, or (c) 45% PEG2000-(EEKKK)₃E. (d) Quantification of colocalization between micelles and megalin. Scale bar: 100 μ m. * $p < .05$, ** $p < .01$



(1000)-amine/DSPE-PEG(2000)-amine/ DSPE-PEG(5000)-amine (Avanti Polar Lipids, Alabaster, AL) in 0.1 M sodium bicarbonate solution (pH 8.3) at room temperature overnight. The mixture was purified on a C4 column and characterized by MALDI-TOF as described above.

13 types of micelles were synthesized via self-assembly. Micelles consisting of varying molar ratios of amphiphiles were synthesized: 100% DSPE-PEG-peptide, 50:50 molar ratio of DSPE-PEG-methoxy: DSPE-PEG-peptide, 90:10 molar ratio of DSPE-PEG-peptide:DSPE-PEG-Cy7, and 45:45:10 molar ratio of DSPE-PEG-methoxy:DSPE-PEG-peptide:DSPE-PEG-Cy7. All monomers were dissolved in methanol or chloroform and evaporated with nitrogen to form thin films. Thin films were dried overnight under vacuum and hydrated at 80°C for 30 min. Micelles prepared for DLS, zeta potential measurements, and TEM were hydrated in Milli-Q water, whereas micelles prepared for in vivo administration were hydrated in phosphate buffered saline (PBS).

4.2 | Dynamic light scattering (DLS) and zeta potential measurements

Micelles containing 100% DSPE-PEG-peptide or 50:50 by molar ratio DSPE-PEG-methoxy: DSPE-PEG-peptide were synthesized and assessed

via DLS and zeta potential measurements. Micelle diameter and zeta potential was measured using Zetasizer Ultra (Malvern Instruments, Malvern, UK) at a micelle concentration of 100 μ M in Milli-Q water ($n = 4$) immediately after micelles were hydrated from thin films.

4.3 | Transmission electron microscopy

Seven microliters of 100 μ M micelles solution in Milli-Q water was placed onto a 200-mesh carbon TEM grid (Ted Pella, Redding, CA) for 5 min. Then, the grid was washed with Milli-Q water and negatively stained with 2 wt.% uranyl acetate solution (Polysciences, Warrington, PA). The staining solution was wicked away after 2 min and the grid was washed with Milli-Q water again. The grid was dried overnight under room temperature in the dark and imaged on a JEOL 2100F (JEOL, Tokyo, Japan).

4.4 | In vivo renal targeting and biodistribution

To test the renal targeting ability in vivo, 100 μ l of 1,000 μ M micelles containing 90:10 molar ratio of DSPE-PEG-peptide:DSPE-

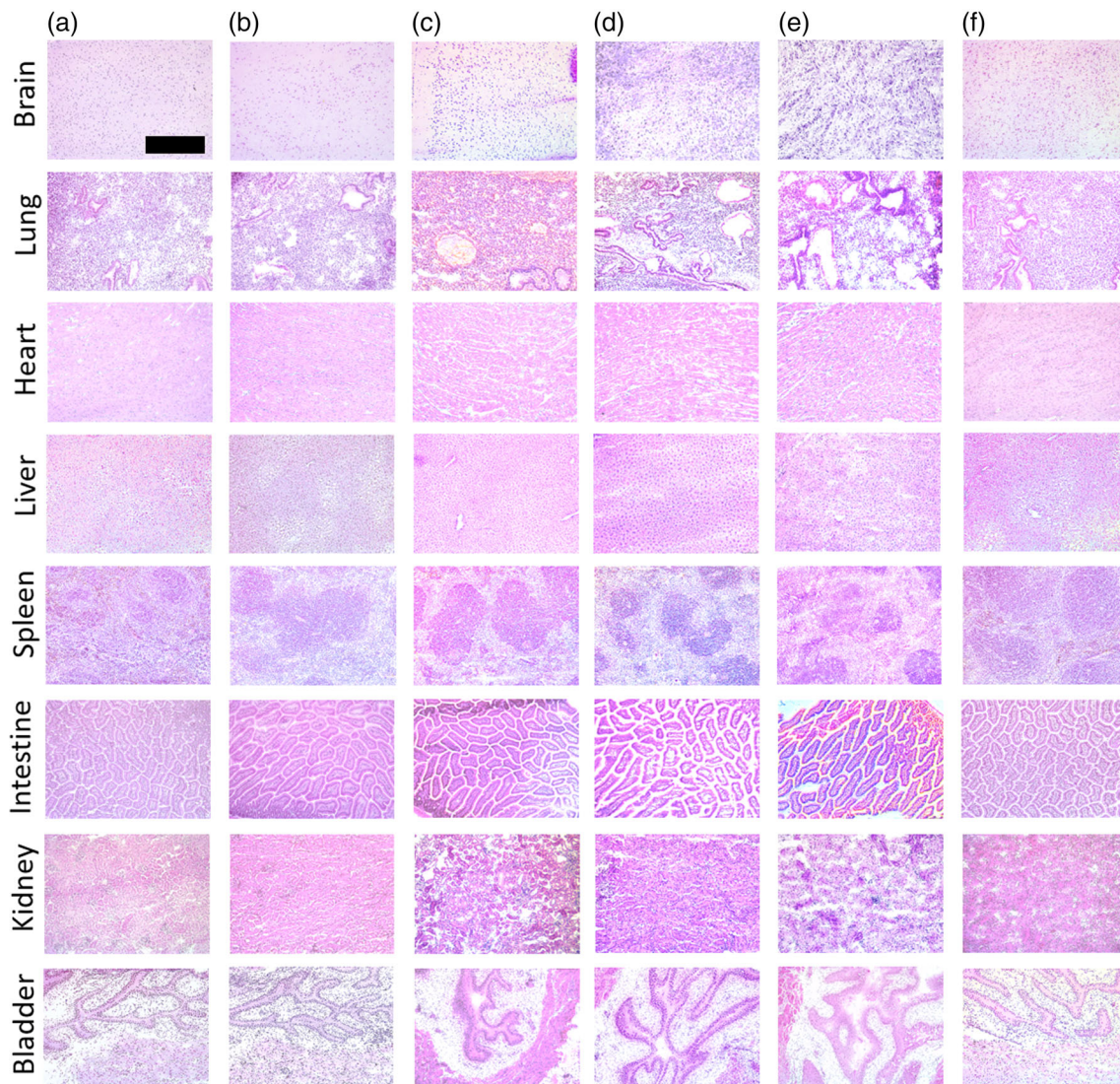


FIGURE 6 H&E staining of kidney sections 24 hr after (a) 45% PEG2000-(KKEEE)₃K, (b) 45% PEG2000-(EEKKK)₃E, (c) 45% PEG2000-KKKKK, (d) 45% PEG2000-EEEE, (e) 90% PEG2000-NT and (f) PBS administration. Scale bar: 100 μ m

PEG-Cy7 or 45:45:10 molar ratio of DSPE-PEG-methoxy:DSPE-PEG-peptide:DSPE-PEG-Cy7 or PBS were tail vein injected with in 6–7 week old male and female C57BL/6 mice ($n = 4$, Jackson Laboratories, Bar Harbor, ME). After 24 hours in circulation, mice were euthanized and their organs (i.e., brain, heart, lungs, liver, spleen, intestines, kidneys, and bladder) were harvested and imaged ex vivo via Ami HTX (Spectral Instruments Imaging, Tucson, AZ). Qualification of the fluorescence signal was conducted to determine the biodistribution of particles by Aura imaging software (Spectral Instruments Imaging, Tucson, AZ). All animal experiments were approved by University of Southern California (USC) Institutional Animal Care and Use Committee (IACUC).

4.5 | Histology

Immediately after ex vivo imaging, harvested organs were flash frozen in 2-methylbutane and liquid nitrogen, embedded in optimum cutting

temperature (OCT) compound, and sectioned into 8 μ m samples via a CM3050 S Cryostat (Leica CM3050S, Leica, Wetzlar, Germany). Tissue sections were then stained with hematoxylin and eosin (H&E) and imaged with a microscope (Leica DMI8, Leica, Wetzlar, Germany).

4.6 | Immunohistochemistry

To assess micelle colocalization with megalin, kidney tissue sections were first washed with Tris buffered saline (TBS) plus 0.025% Triton X-100 with gentle agitation for 10 minutes. A block buffer with 1% bovine serum albumin (BSA), 10% normal goat serum, and 0.3 M glycine in 0.1% PBS Tween was applied to the slides for 1 hour at room temperature. Then, the slides were applied with an anti-Lrp2/Megalin antibody (Abcam, Cambridge, UK, 1:100) overnight at 4°C. The following day, slides were rinsed twice with TBS plus 0.025% Triton for 5 minutes and applied with fluorophore-conjugated secondary antibody-goat, anti-mouse IgG H&L Alexa Fluor® 488 (Abcam, Cambridge, UK, 1:1000) for

TABLE 2 BUN and urine creatinine levels upon micelle administration

NP	BUN (mg/dl)	Creatinine (mg/dl)
45% PEG2000-(KKEEE) ₃ K	40.8 ± 12.6	5.5 ± 1.8
45% PEG2000-(KKEEE) ₂ K	64.6 ± 33.3	5.7 ± 3.1
45% PEG2000-(KKEEE)K	47.9 ± 13.9	4.2 ± 0.2
45% PEG2000-(EEKKK) ₃ E	35.2 ± 8.6	5.5 ± 1.9
45% PEG2000-(EEKKK) ₂ E	60.7 ± 30.4	9.0 ± 3.5
45% PEG2000-(EEKKK)E	48.4 ± 12.8	4.5 ± 2.6
45% PEG2000-KKKKK	41.4 ± 1.6	4.9 ± 0.4
45% PEG2000-EEEE	48.7 ± 4.3	5.6 ± 3.4
90% PEG2000-(KKEEE) ₃ K	29.5 ± 6.8	4.1 ± 1.7
90% PEG2000-(EEKKK) ₃ E	26.3 ± 16.0	3.9 ± 1.2
45% PEG1000-(KKEEE) ₃ K	39.5 ± 4.1	5.0 ± 3.1
90% PEG5000-(KKEEE) ₃ K	54.0 ± 10.9	5.1 ± 1.0
90% PEG2000-NT	36.2 ± 5.5	4.4 ± 3.9
PBS	47.1 ± 9.4	7.6 ± 5.4

1 hour at room temperature in the dark. Slides were then counterstained with DAPI and mounted with VectaMount™ mounting medium (Vector Laboratories, Burlingame, CA). Fixed slides were imaged with a LSM 700 confocal microscope (Zeiss, Oberkochen, Germany), and the colocalization between Cy7 and Alexa Fluor® 488 channels was performed on ImageJ with coloc2.

4.7 | Kidney health

Renal health was assessed by analyzing blood urea nitrogen and urine creatinine levels in serum and urine. BUN was analyzed by a BUN enzymatic kit (Bio scientific, Austin, TX), and urine creatinine was assessed by a mouse creatinine enzymatic kit (Crystal Chem, Elk Grove Village, IL).

4.8 | Statistical analysis

All statistical analyses were performed using GraphPad Prism 8 (San Diego, CA). Analysis of variance (ANOVA) with a Tukey's test for post-hoc analysis was used to determine statistical significance and $p \leq .05$ was considered to be significant.

ACKNOWLEDGMENTS

The authors would like to acknowledge the financial support from the Women in Science and Engineering (WiSE), Gabilan Assistant Professorship, L. K. Whittier Foundation, the National Heart, Lung, and Blood Institute (NHLBI, R00HL124279), and NIH New Innovator Award (DP2-DK121328) awarded to E.J.C. TEM images were taken with the aid of USC Center of Excellence in Nano Imaging.

CONFLICT OF INTEREST

The authors declare no potential conflict of interest.

ORCID

Eun Ji Chung  <https://orcid.org/0000-0002-7726-5555>

REFERENCES

- Jha V, Garcia-Garcia G, Iseki K. Chronic kidney disease: global dimension and perspectives (vol 382, pg 260, 2013). *Lancet*. 2013;382(9888):208-208.
- Harris PC, Torres VE. Polycystic kidney disease. *Annu Rev Med*. 2009; 60:321-337.
- Hateboer N, v Dijk MA, Bogdanova N, et al. Comparison of phenotypes of polycystic kidney disease types 1 and 2. European PKD1-PKD2 study group. *Lancet*. 1999;353(9147):103-107.
- Chapman AB, Devuyst O, Eckardt KU, et al. Autosomal-dominant polycystic kidney disease (ADPKD): executive summary from a kidney disease: improving global outcomes (KDIGO) controversies conference. *Kidney Int*. 2015;88(1):17-27.
- Luciano RL, Dahl NK. Extra-renal manifestations of autosomal dominant polycystic kidney disease (ADPKD): considerations for routine screening and management. *Nephrol Dial Transplant*. 2014;29(2): 247-254.
- Chebib FT, Perrone RD, Chapman AB, et al. A practical guide for treatment of rapidly progressive ADPKD with Tolvaptan. *J Am Soc Nephrol*. 2018;29(10):2458-2470.
- Wang A, Hirose T, Ohsaki Y, et al. Hydrochlorothiazide ameliorates polyuria caused by tolvaptan treatment of polycystic kidney disease in PCK rats. *Clin Exp Nephrol*. 2019;23(4):455-464.
- Khan MY, Rawala MS, Siddiqui M, Abid W, Aslam A. Tolvaptan-induced liver injury: who is at risk? A case report and literature review. *Cureus*. 2019;11(6):e4842.
- Torres VE, Chapman AB, Devuyst O, et al. Tolvaptan in patients with autosomal dominant polycystic kidney disease. *N Engl J Med*. 2012; 367(25):2407-2418.
- Cardenas A, Ginès P, Marotta P, et al. Tolvaptan, an oral vasopressin antagonist, in the treatment of hyponatremia in cirrhosis. *J Hepatol*. 2012;56(3):571-578.
- Kramers BJ, van Gastel MDA, Meijer E, Gansevoort RT. Case report: a thiazide diuretic to treat polyuria induced by tolvaptan. *BMC Nephrol*. 2018;19(1):157.
- Kramers BJ, van Gastel MDA, Boertien WE, Meijer E, Gansevoort RT. Determinants of urine volume in ADPKD patients using the vasopressin V2 receptor antagonist Tolvaptan. *Am J Kidney Dis*. 2019;73(3): 354-362.
- Chauveau D, Fakhouri F, Grunfeld JP. Liver involvement in autosomal-dominant polycystic kidney disease: therapeutic dilemma. *J Am Soc Nephrol*. 2000;11(9):1767-1775.
- Pellegrino AM, Annicchiarico Petruzzelli L, Riccio E, Pisani A. Idiosyncratic hepatic toxicity in autosomal dominant polycystic kidney disease (ADPKD) patient in combined treatment with tolvaptan and amoxicillin/clavulanic acid: a case report. *BMC Nephrol*. 2019;20(1):426.
- Blair HA. Tolvaptan: a review in autosomal dominant polycystic kidney disease. *Drugs*. 2019;79(3):303-313.
- Belaiche S, Romanet T, Allenet B, Calop J, Zaoui P. Identification of drug-related problems in ambulatory chronic kidney disease patients: a 6-month prospective study. *J Nephrol*. 2012;25(5):782-788.
- Ostermann M, Palchaudhuri P, Riding A, Begum P, Milburn HJ. Incidence of tuberculosis is high in chronic kidney disease patients in south East England and drug resistance common. *Ren Fail*. 2016;38(2):256-261.

18. Wischnjow A, Sarko D, Janzer M, et al. Renal targeting: peptide-based drug delivery to proximal tubule cells. *Bioconjug Chem*. 2016;27(4):1050-1057.
19. Wang J, Poon C, Chin D, et al. Design and in vivo characterization of kidney-targeting multimodal micelles for renal drug delivery. *Nano Res*. 2018;11(10):5584-5595.
20. Janzer M, Larbig G, Kübelbeck A, Wischnjow A, Haberkorn U, Mier W. Drug conjugation affects pharmacokinetics and specificity of kidney-targeted peptide carriers. *Bioconjug Chem*. 2016;27(10):2441-2449.
21. Choi CH, Zuckerman JE, Webster P, Davis ME. Targeting kidney mesangium by nanoparticles of defined size. *Proc Natl Acad Sci U S A*. 2011;108(16):6656-6661.
22. Miner JH. Glomerular basement membrane composition and the filtration barrier. *Pediatr Nephrol*. 2011;26(9):1413-1417.
23. Liu GW, Prossnitz AN, Eng DG, et al. Glomerular disease augments kidney accumulation of synthetic anionic polymers. *Biomaterials*. 2018;178:317-325.
24. Du BJ, Yu MX, Zheng J. Transport and interactions of nanoparticles in the kidneys. *Nat Rev Mater*. 2018;3(10):358-374.
25. Morita H, Yoshimura A, Kimata K. The role of heparan sulfate in the glomerular basement membrane. *Kidney Int*. 2008;73(3):247-248.
26. Li L, Bonventre JV. Endothelial Glycocalyx: not just a sugar coat. *Am J Respir Crit Care Med*. 2016;194(4):390-393.
27. Uchimido R, Schmidt EP, Shapiro NI. The glycocalyx: a novel diagnostic and therapeutic target in sepsis. *Crit Care*. 2019;23(1):16.
28. Miner JH. The glomerular basement membrane. *Exp Cell Res*. 2012;318(9):973-978.
29. Chew C, Lennon R. Basement membrane defects in genetic kidney diseases. *Front Pediatr*. 2018;6:1-16.
30. Ning X, Peng C, Li ES, et al. Physiological stability and renal clearance of ultrasmall zwitterionic gold nanoparticles: ligand length matters. *APL Mater*. 2017;5(5):1-7.
31. Ahrabi AK, Jouret F, Marbaix E, et al. Glomerular and proximal tubule cysts as early manifestations of Pkd1 deletion. *Nephrol Dialysis Transplant*. 2010;25(4):1067-1078.
32. Galarreta CI, Grantham JJ, Forbes MS, Maser RL, Wallace DP, Chevalier RL. Tubular obstruction leads to progressive proximal tubular injury and Atubular glomeruli in polycystic kidney disease. *Am J Pathol*. 2014;184(7):1957-1966.
33. Chung EJ, Cheng Y, Morshed R, et al. Fibrin-binding, peptide amphiphile micelles for targeting glioblastoma. *Biomaterials*. 2014;35(4):1249-1256.
34. Kastantin M, Ananthanarayanan B, Karmali P, Ruoslahti E, Tirrell M. Effect of the lipid chain melting transition on the stability of DSPE-PEG(2000) micelles. *Langmuir*. 2009;25(13):7279-7286.
35. Chung EJ, Mlinar LB, Nord K, et al. Monocyte-targeting supramolecular micellar assemblies: a molecular diagnostic tool for atherosclerosis. *Adv Healthc Mater*. 2015;4(3):367-376.
36. Zuckerman JE, Choi CHJ, Han H, Davis ME. Polycation-siRNA nanoparticles can disassemble at the kidney glomerular basement membrane. *Proc Natl Acad Sci U S A*. 2012;109(8):3137-3142.
37. Pombo Garcia K, Zarschler K, Barbaro L, et al. Zwitterionic-coated "stealth" nanoparticles for biomedical applications: recent advances in countering biomolecular corona formation and uptake by the mononuclear phagocyte system. *Small*. 2014;10(13):2516-2529.
38. Murthy AK, Stover RJ, Hardin WG, et al. Charged gold nanoparticles with essentially zero serum protein adsorption in undiluted fetal bovine serum. *J Am Chem Soc*. 2013;135(21):7799-7802.
39. Liu W, Choi HS, Zimmer JP, Tanaka E, Frangioni JV, Bawendi M. Compact cysteine-coated CdSe(ZnCdS) quantum dots for in vivo applications. *J Am Chem Soc*. 2007;129(47):14530-14531.
40. Kane RS, Deschatelets P, Whitesides GM. Kosmotropes form the basis of protein-resistant surfaces. *Langmuir*. 2003;19(6):2388-2391.
41. Piatkovsky M, Acar H, Marciel AB, Tirrell M, Herzberg M. A zwitterionic block-copolymer, based on glutamic acid and lysine, reduces the biofouling of UF and RO membranes. *J Membr Sci*. 2018;549:507-514.
42. Owens DE 3rd, Peppas NA. Opsonization, biodistribution, and pharmacokinetics of polymeric nanoparticles. *Int J Pharm*. 2006;307(1):93-102.
43. Estephan ZG, Jaber JA, Schlenoff JB. Zwitterion-stabilized silica nanoparticles: toward nonstick nano. *Langmuir*. 2010;26(22):16884-16889.
44. Holmlin RE, Chen X, Chapman RG, Takayama S, Whitesides GM. Zwitterionic SAMs that resist nonspecific adsorption of protein from aqueous buffer. *Langmuir*. 2001;17(9):2841-2850.
45. Liang X, Wang H, Zhu Y, et al. Short- and long-term tracking of anionic ultrasmall nanoparticles in kidney. *ACS Nano*. 2016;10(1):387-395.
46. Balogh L, Nigavekar SS, Nair BM, et al. Significant effect of size on the in vivo biodistribution of gold composite nanodevices in mouse tumor models. *Nanomedicine*. 2007;3(4):281-296.
47. Comper WD, Glasgow EF. Charge selectivity in kidney ultrafiltration. *Kidney Int*. 1995;47(5):1242-1251.
48. Perry MA, Benoit JN, Kviety PR, Granger DN. Restricted transport of cationic macromolecules across intestinal capillaries. *Am J Physiol*. 1983;245(4):G568-G572.
49. Xiao K, Li Y, Luo J, et al. The effect of surface charge on in vivo biodistribution of PEG-oligocholeic acid based micellar nanoparticles. *Biomaterials*. 2011;32(13):3435-3446.
50. LaConte LE, Nitin N, Zurkiya O, et al. Coating thickness of magnetic iron oxide nanoparticles affects R2 relaxivity. *J Magn Reson Imaging*. 2007;26(6):1634-1641.
51. Tauris J, Christensen EI, Nykjær A, Jacobsen C, Petersen CM, Ovesen T. Cubilin and megalin co-localize in the neonatal inner ear. *Audiol Neurootol*. 2009;14(4):267-278.
52. Christensen EI, Birn H. Megalin and cubilin: multifunctional endocytic receptors. *Nat Rev Mol Cell Biol*. 2002;3(4):256-266.
53. Christensen EI, Birn H, Verroust P, Moestrup SK. Megalin-mediated endocytosis in renal proximal tubule. *Ren Fail*. 1998;20(2):191-199.
54. Vegt E, Melis M, Eek A, et al. Renal uptake of different radiolabelled peptides is mediated by megalin: SPECT and biodistribution studies in megalin-deficient mice. *Eur J Nucl Med Mol Imaging*. 2011;38(4):623-632.
55. Chung EJ, Mlinar LB, Sugimoto MJ, Nord K, Roman BB, Tirrell M. In vivo biodistribution and clearance of peptide amphiphile micelles. *Nanomedicine*. 2015;11(2):479-487.
56. Chin DD, Poon C, Trac N, et al. Collagenase-cleavable peptide Amphiphile micelles as a novel Theranostic strategy in atherosclerosis. *Adv Therap*. 2020;3(3):1-12.
57. Chin DD, Wang J, de Fontenay MM, Plotkin A, Magee GA, Chung EJ. Hydroxyapatite-binding micelles for the detection of vascular calcification in atherosclerosis. *J Mater Chem B*. 2019;7(41):6449-6457.
58. Poon C, Chowdhuri S, Kuo C-H, et al. Protein mimetic and anticancer properties of monocyte-targeting peptide Amphiphile micelles. *ACS Biomater Sci Eng*. 2017;3(12):3273-3282.
59. Poon C, Gallo J, Joo J, Chang T, Bañobre-López M, Chung EJ. Hybrid, metal oxide-peptide amphiphile micelles for molecular magnetic resonance imaging of atherosclerosis. *J Nanobiotechnol*. 2018;16:1-11.
60. Rodrigues WF, Miguel CB, Napimoga MH, Oliveira CJF, Lazo-Chica JE. Establishing standards for studying renal function in mice through measurements of body size-adjusted creatinine and urea levels. *Biomed Res Int*. 2014;2014:872827.
61. Dunn SR, Qi Z, Bottinger EP, Breyer MD, Sharma K. Utility of endogenous creatinine clearance as a measure of renal function in mice. *Kidney Int*. 2004;65(5):1959-1967.

62. Li M, Corbelli A, Watanabe S, et al. Three-dimensional podocyte-endothelial cell co-cultures: assembly, validation, and application to drug testing and intercellular signaling studies. *Eur J Pharm Sci.* 2016;86:1-12.

SUPPORTING INFORMATION

Additional supporting information may be found online in the Supporting Information section at the end of this article.

How to cite this article: Huang Y, Jiang K, Zhang X, Chung EJ. The effect of size, charge, and peptide ligand length on kidney targeting by small, organic nanoparticles. *Bioeng Transl Med.* 2020;5:e10173. <https://doi.org/10.1002/btm2.10173>